LARGE-SCALE FIELD TESTING OF GEOTECHNICAL SEISMIC ISOLATION OF STRUCTURES USING GRAVEL-RUBBER MIXTURES

Dimitris Pitilakis[1], Anastasios Anastasiadis[1], Athanasios Vratsikidis[1], Anastasios Kapouniaris[1] , Maria Rossella Massimino[2], Glenda Abate[2], Sebastiano Corsico[2]

[1]Department of Civil Engineering, Aristotle University of Thessaloniki, Thessaloniki, Greece
[2]Department of Civil Engineering and Architecture, University of Catania, Catania, Italy

Corresponding Author: Dimitris Pitilakis, dpitilakis@civil.auth.gr, Aristotle University of Thessaloniki

We present the results of a large-scale experimental campaign performed on the prototype structure of EuroProteas in Thessaloniki, Greece, to assess the effectiveness of gravel-rubber mixture (GRM) layers underneath shallow foundations as a means of geotechnical seismic isolation (GSI). We found that the geotechnical seismic isolation of structures is optimized by increasing the rubber content of the soil rubber mixture up to 30% per mixture weight. Although the effectiveness of the GSI systems has been investigated numerically and in small-scale experiments, this paper seeks to fill the gap in the lack of full-scale experimental studies on this subject. Three soil pits were excavated and backfilled with GRM of different rubber content per weight to serve as foundation soil for the structure. A large number of instruments were installed on the structure, the foundation, the soil surface, and inside the gravel-rubber mixture layers beneath the foundation to fully monitor the GSI-structure systems' response in three dimensions. The experimental investigation included ambient noise, free- and forced-vibration tests. Our results showed that a geotechnical seismic isolation layer composed of a gravel-rubber mixture with 30% rubber content per weight effectively isolates the structure. Even 0.5m thickness (i.e., B/6 of the foundation width) of the GSI system is successfully cutting off practically all emitted waves at a (horizontal or vertical) distance of B/6 from the foundation. A significant reduction in the GSI-structure system's stiffness was apparent, leading to a rocking-dominant response. The rise in the system's damping and the substantial energy dissipation inside the GRM layer highlight its effectiveness as a geotechnical seismic isolation system.

KEYWORDS

Geotechnical seismic isolation, gravel-rubber mixtures, experimental soil-structure interaction, field testing, large scale testing

INTRODUCTION

Over the last decades, seismic isolation has been adopted and widely used as an effective strategy in the earthquake resistant design of structures. Seismic isolation systems intend to reduce the earthquake-induced structural damage by decoupling the structure's horizontal motion from the ground shaking and, therefore, modifying the structure's dynamic response. Different systems are used to isolate structures, such as elastomeric bearings, sliding elements, and friction–pendulum systems [1,2]. Their use is emerging as the modern performance-based seismic design of structures takes over the traditional capacity spectrum design. However, their installation and maintenance are considered quite expensive economically and technically for conventional buildings, whereas these solutions are almost prohibited in developing countries where the financial resources are limited.

The urge for alternative low-cost seismic isolation systems has led to various novel designs [3]. Many researchers investigated fully coupled soil-structure isolation systems [4–7] and proposed exploiting the soil's nonlinear behavior and its deformability as a means of natural passive isolation mechanism [8,9]. Although rocking isolation mechanisms have been proven quite successful in the attenuation of motions through soil yielding below the foundations, foundation rocking, uplift, and sliding [10–12], the residual differential settlement after a strong earthquake that requires a realignment of the structure afterward can be considered a drawback. To overcome this challenge, geotechnical seismic isolation (GSI) [13] emerged as a new technique for protecting the structures in earthquake-prone areas. The main idea is to improve the foundation soil so that seismic energy will be partially dissipated within it before being transmitted to the structure.

Among other materials proposed for the foundation soil improvement, soil rubber mixtures (SRM) [13] have attracted significant research interest. SRM, which have been recently included in ASTM and CEN standards [14,15], are characterized by low specific weight, high elasticity, low shear modulus, and high damping [16–22]. Therefore, the use of SRM is advantageous due to their good static and dynamic properties. Simultaneously, the effects of the soil-foundation-structure interaction (SFSI) and rocking isolation are also considered.

Rubber grains for the mixtures are usually manufactured from scrap tires, the disposal of which has become a severe environmental problem worldwide over the last years [23,24]. Consequently, the use of granulated rubber as a construction material has immediate advantageous ecological effects. At the same time, it is considered an affordable alternative for the seismic isolation of conventional structures, especially in developing countries. Besides, recycled rubber in pure form or mixed with soil is proposed in the construction industry in many applications. Granulated tire rubber has been studied numerically [25,26] or experimentally [27] as a lightweight backfill material to reduce the lateral earth pressures on retaining walls. Moreover, the use of tire shreds was proposed in the design of embankments overlying soft soils to minimize the vertical stresses and settlements [24,28] and have been investigated experimentally in constructing a drainage layer based on their high hydraulic conductibility [29,30].

SRM suitability and advantages as GSI in the form of a layer underlying the foundation of a structure have been investigated numerically by many researchers [13,31–38], demonstrating the decrease of the foundation's horizontal and vertical motions. Additionally, it was stated that the low modulus of the SRM foundation layer contributes to the reduction of the rocking stiffness of the structures.

On the other hand, only a few experimental studies on this subject are available in the literature, and they are limited mostly to laboratory and small-scale testing. Kaneko et al. conducted a pseudo-dynamic (hybrid) test to examine the positive effects of SRM in the seismic isolation of structures and prevent liquefaction [39]. Shaking table tests performed on rigid blocks founded on SRM showed that the structural motion was substantially declined by increasing the SRM layer thickness or the rubber proportion in the mixture [40,41]. Tsiavos et al. [42] investigated the sliding response of structures founded on SRM layers with different mean size ratios and thickness, while the sliding interface material was also examined. Furthermore, another shaking table experimental series highlighted the beneficial effects of the SRM in the vibration isolation of structures. [27]. The first centrifuge test on a model structure founded on SRM pronounced increased seismic energy dissipation through sliding and rocking and a resulting structural demand reduction [43]. Relatively fewer field tests concerning the seismic isolation capability of the SRM-filled sleeve piles and trench barriers have been reported [44].

Although the laboratory-scale experiments provide significant insight concerning the behavior of SRM as a GSI strategy, there are certain limitations in reproducing realistic boundary conditions and stress fields in the mixture or the underlying soil and capturing the attenuation of the motion. Large-scale field tests of SRM as a seismic isolation layer beneath full-scale structures are necessary to investigate the SRM-foundation-structure systems' response.

We present the first experimental campaign results on a full-scale prototype structure founded on gravel rubber mixtures (GRM). As a notation, we will use throughout the text the acronym GRM as is, regardless if it expresses singular or plural nouns. Ambient noise was recorded, and free-, and forced-vibration tests were carried out on the structure of EuroProteas located in the Euroseistest experimental facility (http://euroseisdb.civil.auth.gr) after replacing the foundation soil with three different GRM. This study investigates the rubber content effect of the GRM layer on the dynamic response and the overall performance of the GRM as a GSI system. Our results show that a geotechnical seismic isolation layer composed of a gravel-rubber mixture with 30% rubber content per weight effectively isolates the structure

EUROPROTEAS EXPERIMENTAL FACILITY

Test structure

EuroProteas (Figure 1) prototype structure (http://euroseisdb.civil.auth.gr/sfsi) was designed and constructed as a simple test structure that promotes the SFSI phenomena very at the Euroseistest facility, 30km NE of the city of Thessaloniki in Greece. Its large superstructure mass in conjunction with the soft foundation soil promotes SFSI effects and soil's nonlinear behavior during the soil-structure system's excitation. EuroProteas serves as an ideal structure for full-scale testing on SFSI and wave propagation.

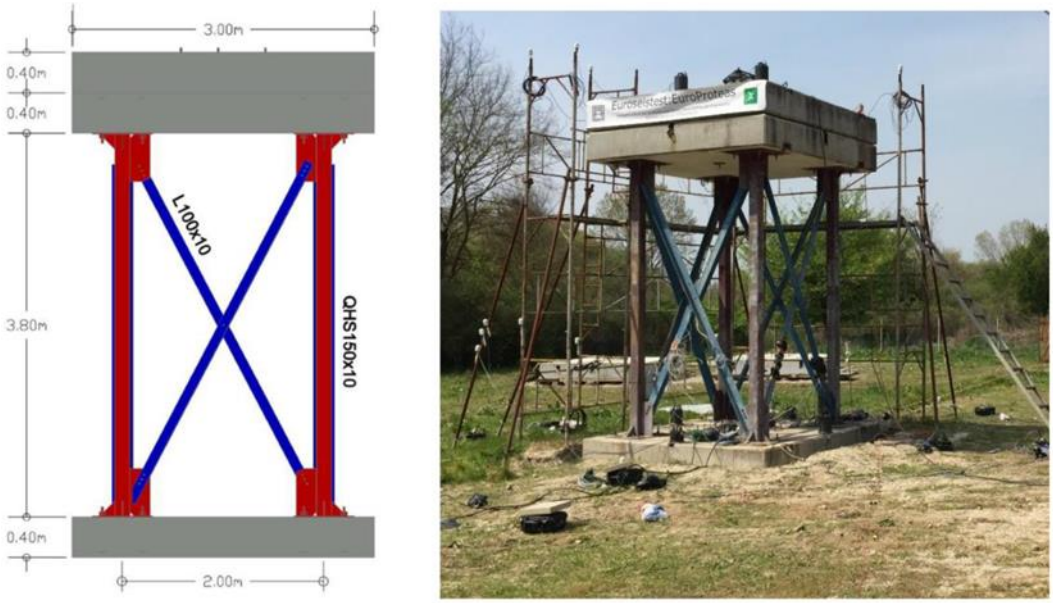

Figure 1 (a) A 2D sketch and (b) a photo of EuroProteas

EuroProteas is founded on a reinforced concrete slab (C20/25) of dimensions 3.00×3.00×0.40m. Four steel columns of section QHS150×150×10mm clamped on the foundation support two identical reinforced concrete slabs forming the superstructure. The columns are connected with steel X-braces of section L100×100×10mm in all directions to ensure the structure's symmetry. Each slab's total mass is estimated at around 9.16Mg, assuming a uniform unit weight of 25kN/m3 for the concrete. The total mass of the structure is calculated approximately at 28.5Mg. The structure's outer dimensions are 3.0×3.0×5.0m. More details on the prototype's design and construction can be found in [45,46].

As the X-braces and the upper roof slab of the superstructure are removable, the modification of its mass and stiffness is optional. Depending on the arrangement of the X-bracing system and the number of the roof slabs, the fixed-base frequency of EuroProteas can vary between 1.78Hz and 13.06Hz as calculated numerically [45]. In the experimental series presented in this paper, the configuration of EuroProteas involved X-bracing in all four sides and two roof slabs yielding to a fixed-base fundamental natural frequency at 9.13Hz.

Foundation soil

Natural Soil

The soil stratigraphy and its physical and dynamic properties at the Euroseistest experimental facility center have been extensively investigated with earlier geophysical and geotechnical studies [47,48]. Before constructing EuroProteas, additional geotechnical and geophysical surveys, including drilling boreholes, Down-Hole tests, resonant column, and cyclic triaxial tests on undisturbed soil samples, were carried out to define in detail the stratigraphy immediately below the foundation [45].

The soil profile below EuroProteas consists of a 7m thick upper layer of silty clayey sand, which overlies a layer of clayey to silty sand with gravels between 7m and 22m and, after that, a layer of marly silt to silty sand until the depth of 30m (Figure 2a). The shear wave velocity of the uppermost 5m varies from 100m/s to 150m/s and then increases to more than 250m/s at 25m depth (Figure 2b).

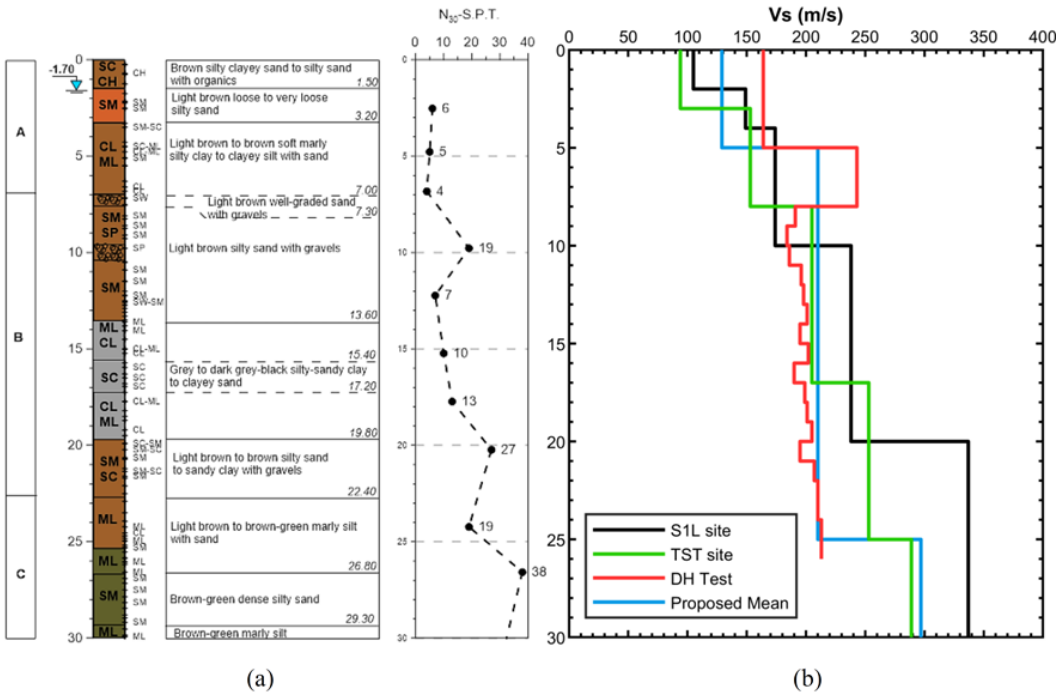

Figure 2 (a) Soil stratigraphy of the 30m deep borehole at the geometrical center of the foundation and (b) V_s profile from down-hole tests (DH Test) compared with V_s profile at S1L site 50m south of EuroProteas, a reference mean V_s model of the valley cross-section and the proposed in [47] **V_s profile at the TST site.**

In the experimental series presented here, we replaced the uppermost 0.5m of the foundation soil with three different GRM backfills. To investigate the influence of the rubber content in the response of the soil-GRM-foundation-structure system, we defined the rubber content per mixture weight (p.w.) 0%, 10%, and 30% for the three foundation mixtures (corresponding to 0%, 25% and 75% per mixture volume respectively).

Improved soil with GRM for GSI

Before improving the foundation soil, a preliminary study was carried out at the Laboratory of Soil Mechanics, Foundations and Geotechnical Earthquake Engineering of the Aristotle University of Thessaloniki to define the physical properties of the three GRM mixtures for the foundation soil improvement.

GRM exhibit lower unit weight compared to natural soils, while their elasticity is higher [24,49,50]. Their dynamic characteristics are quite attractive as the small strain shear modulus takes lower values than typical granular soils, whereas the opposite is observed for the small-strain damping [16–18,21,51]. Additionally, the stiffness degradation and the damping increase exhibit a more linear behavior in the medium and high-strain ranges than natural soils. The behavior is becoming even more linear with increasing rubber content [18].

The relative ratio of the soil-rubber mixture's mean grain size is a critical parameter for the mixture's behavior [18,20,21]. We studied uniform quarry gravel with angular particles fraction of mean grain size $D_{50,G}$ equal to 20.76mm as primary physical material (G). In contrast, a coarse fraction of rubber of mean grain size $D_{50,R}$ equal to 3.27mm was studied as primary synthetic material (R) (Figure 3). As the ratio $D_{50,R}/ D_{50,G}$ is less than unity, we expected a small increase in the mixture's rubber content would lead to a more rubber-like behavior of the GRM [18,20,52]. According to the ASTM D854-02 specification [53], the specific gravity of soil solids, Gs, was found equal to 2.67 for the gravel fraction and 1.10 for the rubber fraction.

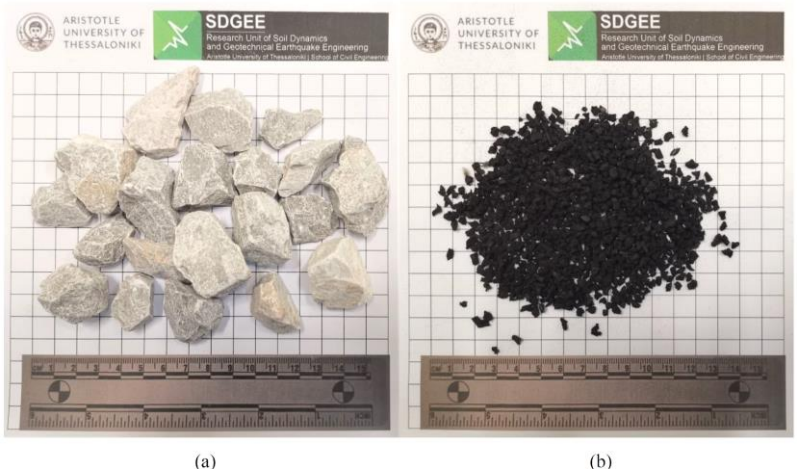

Figure 3 (a) Gravel and (b) rubber materials used in the experiments.

The examined pure gravel specimens and the GRM exhibited "loose sand behavior" without reaching positive volumetric strain values when the axial deformation varied in a range up to 20% [54]. The majority of the examined specimens presented a contractive behavior with a tendency of reduction as the axial deformation increased, regardless of the uniformity of the sample, the particle size, and the relative ratio $D_{50,R}/ D_{50,G}$ of the mean diameter of its granules. However, as the rubber percentage in the mixture increased, or as the level of the applied envelope stress increased, the specimens exhibited a more intense contractive behavior, meaning that the addition of the rubber in the mixture leads to a reduction of the dilation angle values. This behavior is attributed to the high compression and contraction of the soil structure during the consolidation stage because of the high level of the applied radial stress and the high deformability of the rubber granules. Therefore, during the failure stage, the rubber grains, as part of the solid sample structure, had a small margin of deformation left. In contrast, the solid structure in which the soil grains participated was partly rearranged.

Table 1 summarizes the physical characteristics of the natural gravely soil and the synthetic material used in this research. Simultaneously, Figure 4 shows the grain size distribution of the used materials that affect the examined samples' mechanical properties. All of the parameters were determined according to the specification ASTM C136 [55]. The classification of the used physical soils and synthetic materials was performed by the D2487-00 [56] and by the D6270-98 [57] ASTM specifications, respectively.

Table 1 Grain size characteristics and classification of materials used in the experiments.

Properties	Gravel	Rubber
Material ID	G	R
G_s	2.67	1.10
D_{10} (mm)	14.69	2.07
D_{30} (mm)	18.80	2.67
D_{50} (mm)	20.76	3.27
D_{60} (mm)	21.67	3.56
C_u	1.48	1.72
C_c	1.11	0.97
e_{max}	1.385	1.616
e_{min}	0.844	1.075
USCS Classification	GP	Granulated Rubber

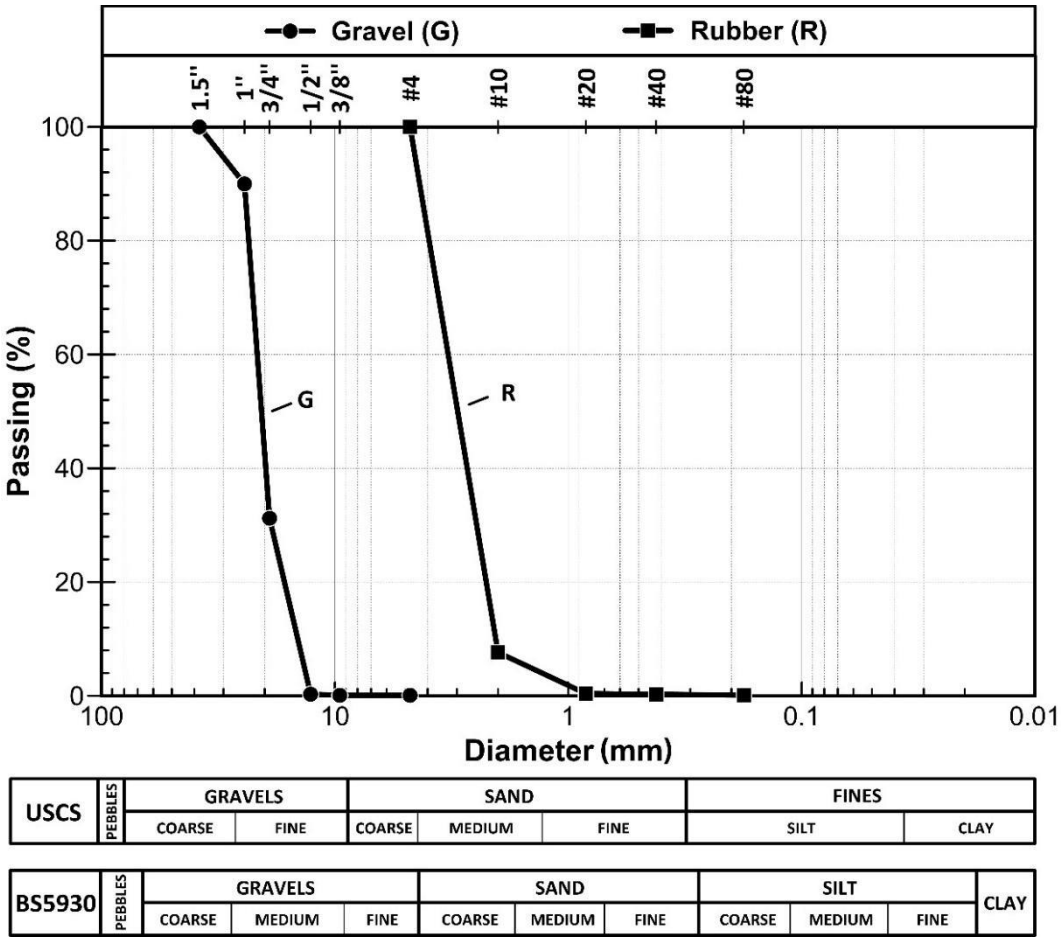

Figure 4 Grain size distribution curves of the gravel (G) and the rubber (R) materials used in the experiments.

Installation of GSI on site

The preparation of the area where the experiments were carried out began with the excavation of three square-plan pits in predetermined positions. With an excavator, three 3.2x3.2m square-plan pits were excavated down to 0.5m depth. A thin geotextile layer was placed to cover the base and the pit walls to prevent the GSI from mixing with the underlying and surrounding fine-grained soil material. The first soil pit was filled only with gravel (i.e., 0% rubber content) to serve as a benchmark GSI case (Figure 5a and 5d). The other two pits were filled with GRM of 10% and 30% rubber content p.w., respectively (Figure 5b and 5c). We will refer to the three GSI systems herein as GRM100/0, GRM90/10, and GRM70/30 for the three rubber percentages 0, 10, 30%, respectively. The physical properties of the three GRM are presented in Table 2.

The mixing of the two materials was done on-site, in an electrical construction mixer. During mixing the gravel with the rubber, a small amount of water (2-3% per mixture) was added to prevent the rubber grains' segregation and ensure rubber and gravel contact behavior during compaction. The GRM foundation soil was spread in two layers of 0.25m height each. We compacted each layer using a soil compactor roller in the 3.2x3.2m area: the bottom layer was compacted for about 10 minutes, as shown in Figure 5b, whereas the top layer for 13 minutes.

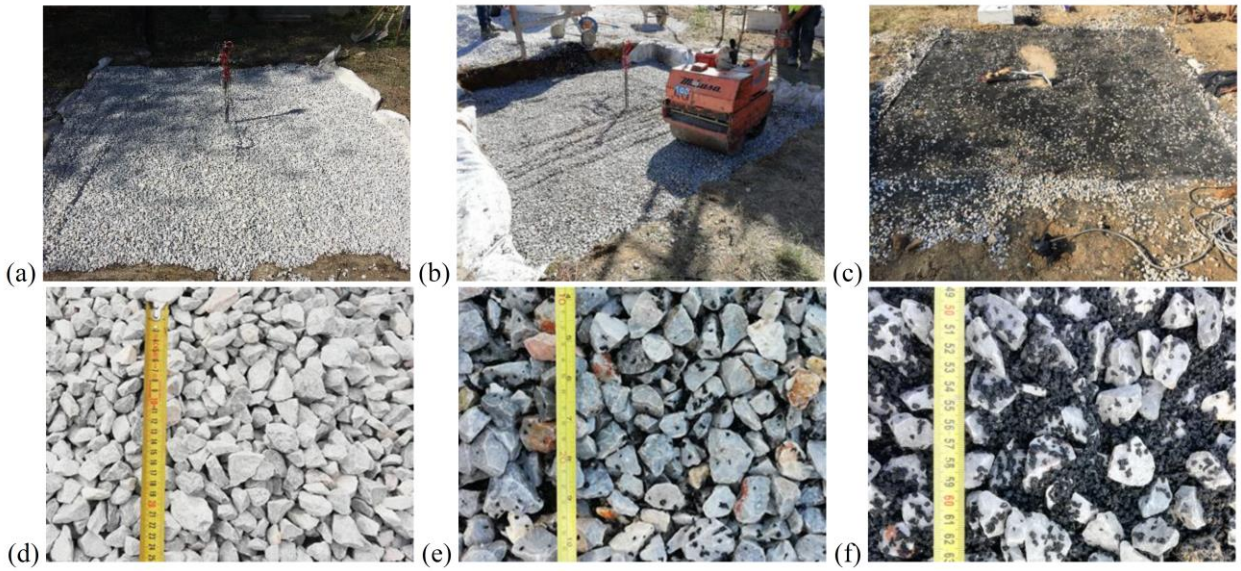

Figure 5 (a) The first soil pit filled with GRM100/0, (b) the second soil pit filled with GRM90/10, (c) the third soil pit filled with GRM70/30 and a detail of the mixtures at each soil pit in (d), (e), (f). A SAAR was installed in the geometrical center of each soil pit until the depth of 1.20m.

Table 2 The foundation soil types used in the experiments.

GRM ID	Rubber content p.w. (%)	$D_{50,R}$ / $D_{50,G}$	G_s	D_r (%)	γ_d (kN/m^3)
GRM100/0	0	-	2.67	98	16.2
GRM90/10	10	0.16	2.51	98	15.2
GRM70/30	30		2.19	59 – 71	11.8

Apart from the pits' instrumentation presented in the next section, a mold with 15.2cm diameter and 17.8cm height was placed inside each pit, at the bottom layer close to the mixture's base. After the end of the test, these molds were carefully removed to calculate some critical parameters such as relative density, water content, void ratio, and verification of the gravel-rubber percentage per weight in the respective pit. An additional identical mold was placed in the third pit in the largest rubber content mixture (GRM70/30) to validate the defined parameters. This mold was placed 0.25m higher, inside the top layer.

We noticed a small discrepancy in the relative density, Dr, of the third mixture, which was higher at the bottom layer even though the conducted compaction tests were identical, and the compaction energy was the same (Table 2). We believe that this is attributed to the poor compaction of the foundation soil near the mold. The proper layering of mixtures consisting of such materials is an essential factor in achieving uniform relative density.

TESTING EQUIPMENT, INSTRUMENTATION, AND DATA ACQUISITION

Testing equipment

A wire rope of 14mm diameter with a nominal strength of 50kN was used to pull-out the superstructure during the free-vibration experiments. The one end of the wire rope was clamped at a 3Mg reinforced concrete counterweight buried in the soil (Figure 6a) and located at 20m away from the three soil pits' geometrical center. The tension to the wire rope was applied by a pulling hoist having a working load limit of 32 kN attached to the counterweight. The other end of the rope was fastened on a steel hook installed on the top roof slab. A load cell inserted between the wire rope and the steel hook measured the applied tension force to the superstructure (Figure 6a).

(a) (b)

Figure 6 (a) The pulling hoist attached to the counterweight and (b) the load cell attached to the roof slab for the application and the measurement of the tension force, respectively.

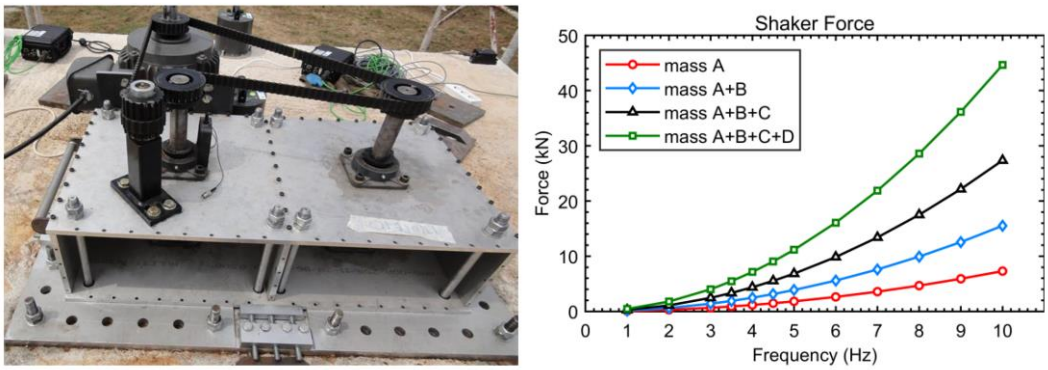

(a) (b)

Figure 7 (a) The eccentric mass shaker MK-500U installed at the geometrical center of the roof and (b) the amplitude of the produced harmonic based on the total eccentricity and the input frequency.

The eccentric mass vibrator system MK-500U (ANCO Engineers Inc.), owned and provided by the Institute of Engineering Seismology and Earthquake Engineering (ITSAK-EPPO), was employed as a source of harmonic excitation for the performance of the forced-vibration experiments (Figure 7a). It is a unidirectional dual counter-rotating shaker that can produce a maximum sinusoidal horizontal force amplitude of 50 kN and can be operated in a frequency range between 0.1Hz and 20Hz at steps of 0.1Hz. Four pairs of plates (A, B, C, and D) in 4 different sizes can be used to modify the vibrator's eccentricity in a range between 0.15kg-m and 11.31kg-m. The output force amplitude is adjusted by the eccentricity and the operating frequency (Figure 7b) according to the following Equation

$$F = E(2\pi f)^2 \quad (1)$$

, where F is the output force (in Newton), E is the eccentricity of the shaker (in kg-m), and f is the rotational speed of the shaker (in Hz).

Instrumentation

We designed a dense instrumentation scheme to monitor and record the response of the structure, the foundation, the GRM layer, and the adjacent soil in three-dimensions (Figure 8). Instrumentation included digital broadband seismometers (CMG-6T and CMG-40T, Guralp Systems Ltd), triaxial accelerometers (Etna2, Kinemetrics Inc. and CMG-5TCDE, Guralp Systems Ltd), Laser Sensors (WayCon Positionsmesstechnik GmbH), Shape Acceleration Arrays (Measurand, Inc.), and Uniaxial Accelerometers (Kistler Holding AG). Instrumentation was made available from the Research Unit of Soil Dynamics and Geotechnical Earthquake Engineering of the Aristotle University of Thessaloniki and the Laboratory of Geophysics of the School of Geology of the Aristotle University of Thessaloniki. The sampling frequency of all the instruments was set at 200 Hz.

Structure monitoring

The structure was instrumented with eight triaxial accelerometers. Four of them were mounted on the roof, two along the axis parallel to the direction of shaking (in-plane) and the other two at the opposite corners of the slab to capture possible out-of-plane motion (Figure 8a). Their positive x-axis was oriented parallel to the positive x-direction of the structure, which forms an angle of 30 degrees with the magnetic North and is parallel to the loading axis in both the free- and forced-vibration tests. The rest of the accelerometers were installed on the foundation slab forming a cross shape to capture the foundation's translational, rocking, and possible out-of-plane motion (Figure 8b).

Moreover, four laser sensors were installed to record the vertical displacement of the foundation slab. These sensors were mounted on two aluminum frames crossing over the foundation slab parallel to the loading axis (Figure 8c, d and e). One laser sensor was also placed at the roof to measure the roof slab's horizontal in-plane motion (Figure 8f).

Soil monitoring

Ten seismometers and one triaxial accelerometer were installed on the soil surface at the foundation base level to monitor the soil response. Eight of the instruments were placed along the loading axis, while the others were placed on the perpendicular axis (Figure 8g). The distance between those close to the structure was defined at 0.50m (=B/6, where B equals the foundation's width). The most distant instrument was installed at 5m (=5B/3).

GRM layer monitoring

A 1.2m shape-acceleration array (SAAR) equipped with eight triaxial MEM sensors every 0.15cm was installed immediately below the foundation's geometrical center to capture the GRM layer's response. Additionally, four uniaxial accelerometers were buried in specific locations under the foundation to fully monitor the response of the GRM (Figure 8f).

Data acquisition and processing

The instruments acquired raw data output in a format that required a conversion in engineering units. Specifically, the accelerometers' raw output is in analog to digital counts, the seismometers and the laser sensors in Volts, and the shape acceleration arrays in m/s^2, m, and Celsius degrees. The converted time series were organized in a separate database. All the recordings were synchronized based on GPS time.

Further processing was necessary before examining the results because of the noise contamination of the recordings. First, the recorded time series were truncated into time windows containing the event of interest and then were zero-padded up to a size equal to a power of 2. This length definition facilitates the frequency domain process, and zero padding is a convenient way to obtain reasonable time series through integration techniques. The time histories were then processed by applying baseline correction and a Tukey window to tapper the edges. Finally, we followed the guidelines recommended in [58] and used a suitable bandpass Butterworth filter with corner frequencies that minimize the low- and high-frequency noise while preserving the frequency range of interest. After integrating in the frequency domain to obtain the displacement response, we judged the chosen filter's appropriateness and its cutoff frequencies. The filtering process was repeated if deemed necessary. The process is presented in the flow chart in Figure 9.

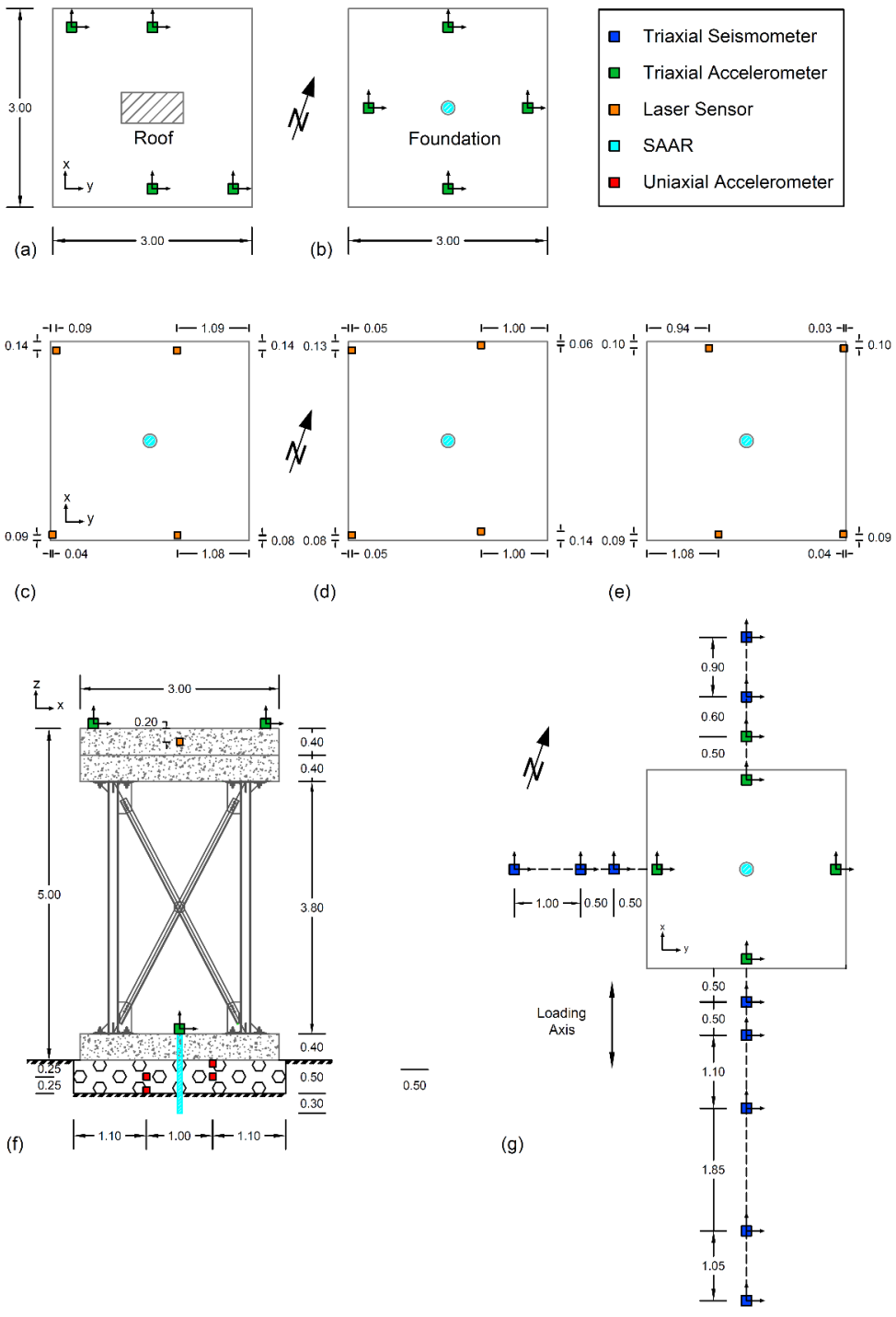

Figure 8 Plan view of the instrumentation of (a) the roof slab (the hatched area indicates the position of the shaker) and (b) the foundation slab with accelerometers. Instrumentation of the foundation slab with laser sensors measuring displacements while resting on the (c) GRM100/0, (d) GRM90/10, and (e) GRM70/30. (f) shows a cross-section of the system and the GRM instrumented with the SAAR and the uniaxial accelerometers and (g) a plan view of the foundation slab and the soil surface instrumented with accelerometers and seismometers.

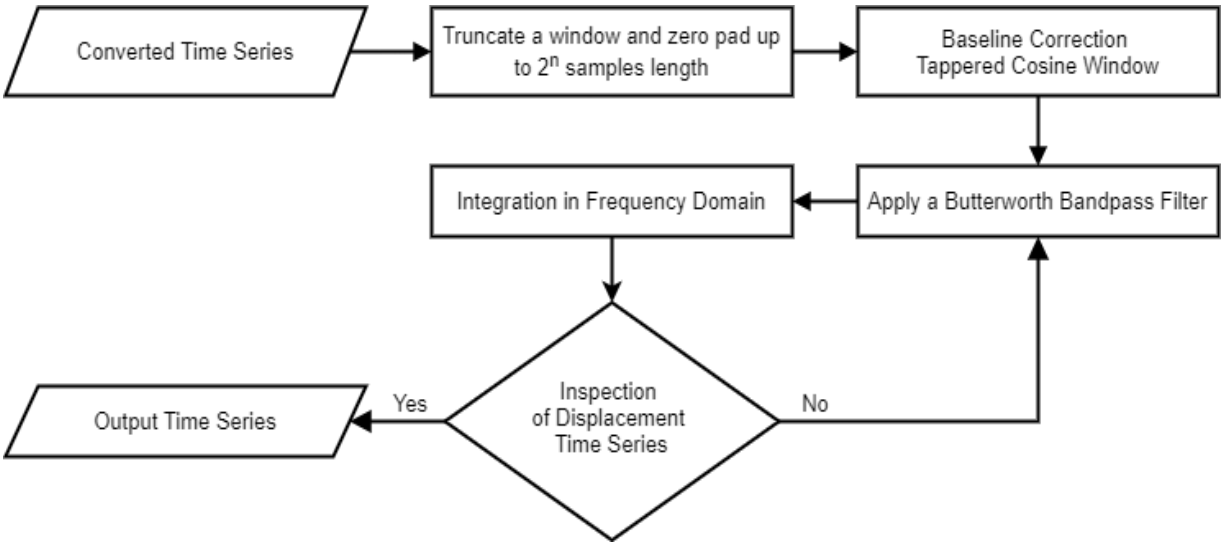

Figure 9 Flowchart of the data processing.

EXPERIMENTAL CAMPAIGN

Ambient noise measurements

Ambient noise measurements provide a convenient means to estimate the dynamic characteristics of a structure without applying any artificial excitation and risking its operation. In this case, environmental noise (wind, steps, etc.) serves as the excitation input to the system. The instruments recorded ambient noise while the structure was sitting on top of each GRM layer before running the free- and forced-vibration test series.

Free-vibration tests

Free-vibration tests are practical dynamic tests that allow the structure to oscillate at its fundamental natural frequency. We carefully designed the free-vibration experiments to capture the structure's response, covering a wide range of pull-out force amplitudes.

Using the equipment described above, when the desired pull-out force was reached by the pulling hoist, the wire rope was cut loose and the structure oscillated freely until rest. In total, 15 pull-out forces varying from 1.35kN to15.20kN were applied to the structure on the three GSI systems (Table 3).

Table 3 Summary of the free-vibration experiments per each GRM configuration.

Experiment ID	Force (kN)		
GRM ID	GRM100/0	GRM90/10	GRM70/30
A	1.60	1.90	1.35
B	10.40	5.40	2.90
C	15.20	10.60	6.28
D	2.10	3.50	9.80
E		7.50	15.00
F		2.80	

Table 4 Summary of the forced-vibration experiments per each foundation soil mixture.

Experiment ID	Mass / Plates	Eccentricity (kg-m)	Frequency Range (Hz)	Force Amplitude (kN)
1	A	1.85	1 – 10	0.07 – 7.30
2	A + B	3.93	1 – 10	0.15 – 15.50
3	A + B + C	6.93	1 – 10	0.30 – 27.30
4	A + B + C + D	11.31	1 – 8	0.50 – 28.50

Forced-vibration tests

The MK-500U eccentric mass shaker was installed at the geometrical center of the roof slab. The produced harmonic force was applied along the structure's principal axis at approximately 30 degrees angle with the magnetic North-South direction (Figure 8a). The performed forced-vibration experiments covered a wide range of excitation amplitude varying from 0.07kN to 28.50kN in a frequency range of 1-10Hz (Table 4) to include the fixed- and flexible-base natural frequencies of all the three GSI-structure systems. The amplitude of the sinusoidal force was calculated by Equation (1), assuming that the mass of the shaker is negligible. The structure was shaken for a time window of 25s at each excitation frequency to reach a steady state. Table 4 summarizes the forced-vibration tests.

EXPERIMENTAL RESULTS

System identification from ambient noise recordings

We applied various system identification techniques on the ambient noise recordings of the instruments installed on the roof and the foundation to estimate the modal parameters of the GSI-structure system. We performed the system identification of the structure using MACEC software [59], a MATLAB-based toolbox that offers various parametric and non-parametric system identification methods. As the environmental ambient input noise is not quantifiable and the actual excitation remains unknown, we implemented the parametric Reference-based covariance-driven Stochastic Subspace Identification (SSI-ref), the non-parametric Peak Picking (PP), and the Frequency Domain Decomposition (FDD) output-only methods. The first method (SSI-ref) provides a direct evaluation of the eigenfrequencies and the modal damping, whereas the other two (PP and FDD) estimate only the modal frequencies.

The first three modes for each GRM configuration are presented in Table 5. The first two modes are identified as translational and the third as torsional in all the GSI-structure systems. The fundamental natural frequencies calculated by each method are almost identical for all the GRM configurations. The modes in the case of GRM100/0 are practically equal to those corresponding to the GRM90/10, indicating that an addition of 10% of rubber content per mixture weight has a marginal influence on the structure's response. On the other hand, when the rubber content per mixture weight increases to 30%, the fundamental natural frequency of the GSI-structure system reduces significantly. This increased rubber content in the GRM layer causes a considerable decrease in the system's stiffness. Furthermore, the estimated damping ratio rises remarkably.

Table 5 Resonant frequencies and damping ratio identified using various system identification methods

GRM ID	Method	SSI-ref		PP	FDD
	Mode	f (Hz)	ζ (%)	f (Hz)	f (Hz)
GRM100/0	1	4.44	1.95	4.44	4.44
	2	4.95	1.17	4.88	4.88
	3	9.69	0.43	9.67	9.67
GRM90/10	1	4.26	1.55	4.30	4.30
	2	4.64	2.49	4.64	4.64
	3	9.41	0.50	9.42	9.42
GRM70/30	1	2.39	5.60	2.44	2.44
	2	2.78	4.93	2.73	2.73
	3	7.14	2.55	7.13	7.13

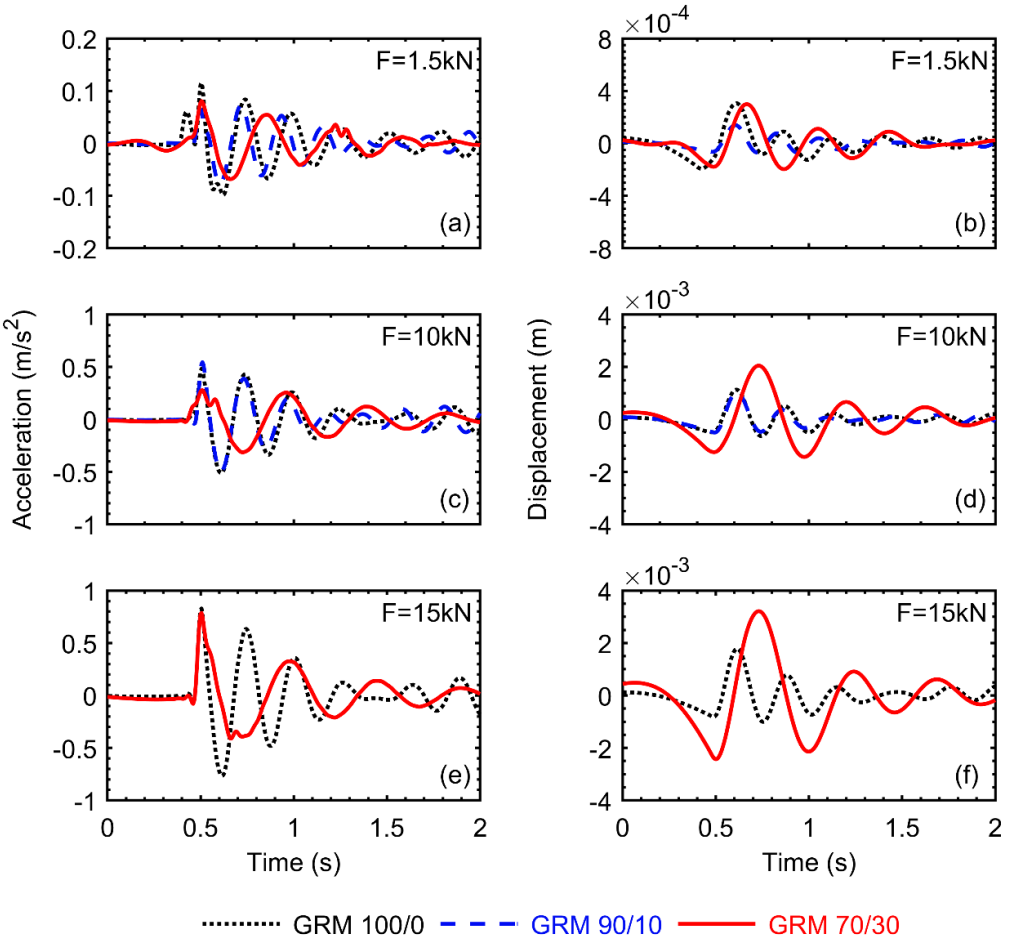

Figure 10 Horizontal roof response in terms of acceleration (a, c, e) and displacement (b, d, f) for pull-out forces of 1.5kN, 10kN, and 15kN, while the structure rests on the three different GRM layers.

Free-vibration results

In Figure 10, we present the horizontal roof translation when the structure is subjected to pull-out forces of amplitude 1.5kN, 10kN, and 15kN, and is placed on the three different GSI layers. The fundamental natural frequencies of the response when EuroProteas rests on the GRM100/0 and GRM90/10 are approximately equal. The presence of only 10% rubber content per weight seems to have a modest effect on modifying the dynamic parameters of the GSI-structure system. Additionally, the amplitude of the roof response in terms of acceleration and displacement is almost the same. This negligible effect of the small rubber proportion on the mixture's dynamic characteristics was also pointed out in earlier laboratory and numerical studies [33,51].

On the other hand, we clearly notice that the increase of the rubber content in the GSI layer to 30% significantly affects the system's corresponding fundamental frequency, which shifts to a lower value indicating a reduction in the system's stiffness. This increase in the fundamental natural period of the GSI-structure system with increasing rubber content per mixture weight confirms our results of the system identification from ambient noise measurements.

Furthermore, in Figure 10, we see that the acceleration response amplitude decrease is more remarkable for the same number of oscillation cycles in the GRM70/30 foundation soil. This decrease is plainly visible in Figure 11, which shows the decay of the recorded acceleration at the roof during the first three oscillation cycles for two different free-vibration experiments. When a small force of 1.5kN is applied, the decay of the recorded acceleration of the structure founded on the GRM70/30 is only slightly larger than the GRM100/0 layer (Figure 11a and b). On the other hand, when the structure is subjected to a larger pull-out force (Figure 11c and d), we notice a decrease in the acceleration

by 60% in the first cycle of oscillation for the GRM70/30. This decrease is more than a twofold reduction compared to the response of the structure founded on the GRM100/0. Moreover, the amplitude of the acceleration of the structure resting on the GRM70/30 in the second cycle is substantially reduced to almost 15% of its initial value, highlighting the rubber's contribution in the damping of the GSI-structure system.

Another important observation in Figure 10 is the increase in the roof displacement during the first cycles of oscillation when the structure is placed on the GRM70/30 layer. To further investigate this outcome, we disassembled the recorded acceleration quantities into their components [60,61]. The foundation rotational acceleration, $\ddot{\theta}_f$, was calculated from the difference of the vertical components of the two accelerometers placed on the foundation edges divided by their intermediate distance, assuming that the foundation slab is rigid. The foundation translational acceleration, $\ddot{u}_f$, is evaluated by removing the term of translational acceleration related to the foundation rotational acceleration ($\ddot{\theta}_f$ multiplied by the foundation slab thickness h_f) from the measured horizontal acceleration at the top of the foundation slab. Finally, the structural translational component because of flexure, $\ddot{u}_s$, is estimated by subtracting from the recorded acceleration the foundation translational acceleration, and the horizontal acceleration quantity related to the foundation rotational acceleration ($\ddot{\theta}_f$ multiplied by the height of the roof mass center h).

In Figure 12, we present the time series of the components for two different free vibration experiments. When the structure is founded on the gravelly soil (GRM100/0), the structural horizontal flexure component ($\ddot{u}_s$) is almost equal to the translational because of the rocking component ($h\ddot{\theta}_f$). A 10% increase of rubber content in the GRM results in a slight difference between the roof horizontal components in favor of the translation produced by rocking. However, when the rubber content increases to 30% of the mixture weight, the horizontal acceleration due to rocking clearly dominates the structure's response, being over three times larger than the horizontal roof response irrespectively of the applied pull-out force. Moreover, as $\ddot{u}_s$ decreases and becomes almost equal to $\ddot{u}_f$, the structure tends to oscillate like a rigid body. Therefore, the observed increased displacement response of the structure is attributed to the rocking-dominant behavior of the GSI-structure system.

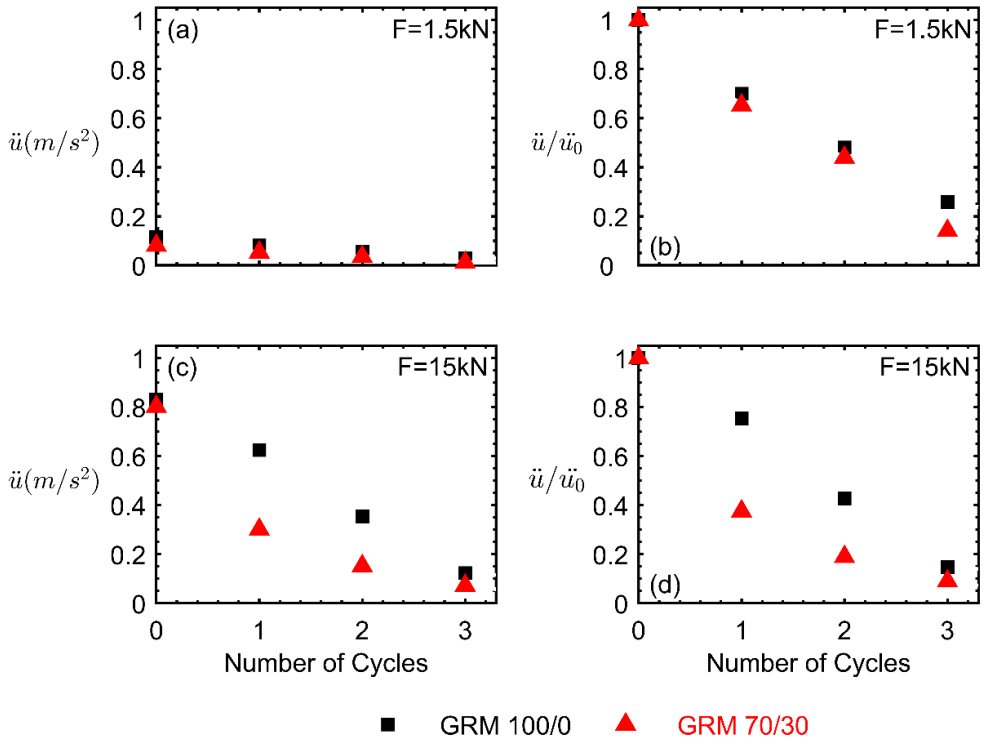

Figure 11 Decay of the roof acceleration as measured (a, c) and normalized by its initial maximum value during the first three cycles of oscillation (b, d) for pull-out force 1.5kN and 15kN, in the case of GRM100/0 and GRM70/30.

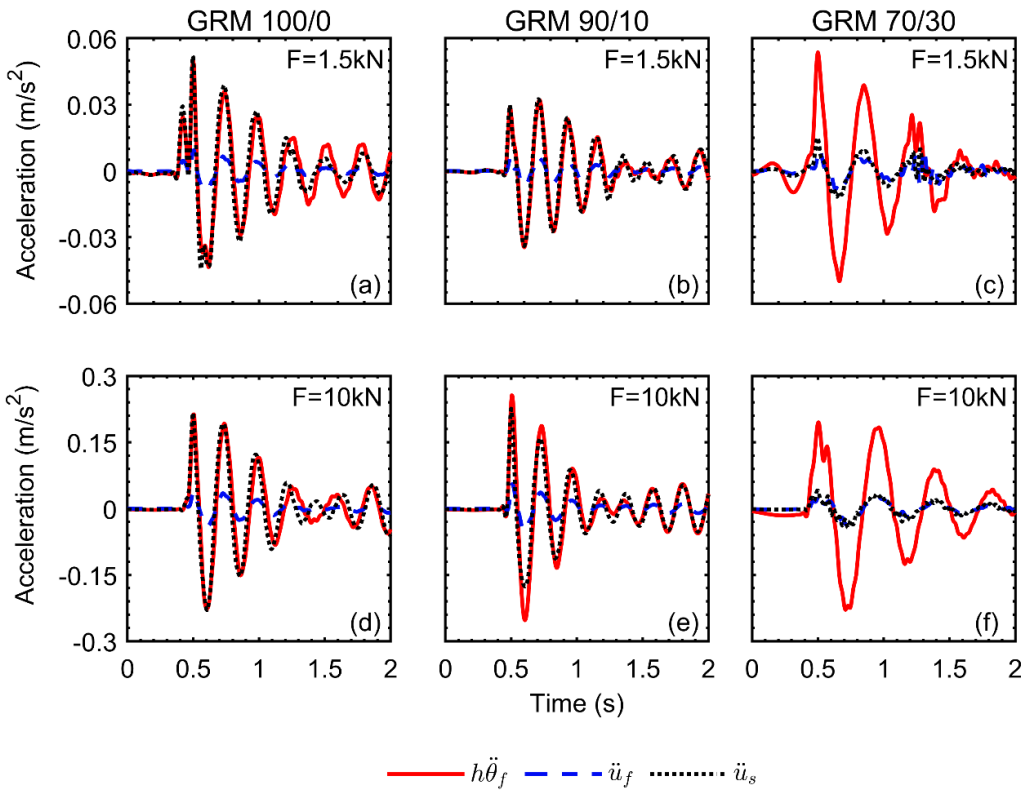

Figure 12 Components of the horizontal roof response during the free-vibration experiments with an applied force of 1.5kN and 10kN while the structure sits on the (a, d) GRM100/0, (b, e) GRM90/10, and (c, f) GRM70/30. $h\ddot{\theta}_f$ is the horizontal acceleration of the roof because of the foundation rocking, $\ddot{u}_f$ is the horizontal acceleration of the foundation, and $\ddot{u}_s$ is the horizontal acceleration of the roof slab because of structural bending.

Figure 13 compares base moment and foundation rotation for pull-out forces of 1.5kN and 15kN in the case of the GRM100/0 and GRM70/30. The base moment was calculated directly by multiplying the inertial force of the roof, i.e., the product of the roof mass and the recorded horizontal roof acceleration, with the distance between the centers of mass of the top and the foundation slab.

When the structure oscillates on the GRM70/30, a significant decrease is evident in the base moment acting on the foundation and a significant simultaneous increase in the foundation rotation, regardless of the applied pull-out force. This moment-rotation behavior results in an apparent reduction in the rocking stiffness in the presence of rubber in the foundation soil, pronouncing the rocking-dominant response of the structure. Additionally, the hysteretic loops have an elliptic shape. They remain relatively narrow, indicating an almost elastic behavior of the GRM and linearity in the structure's response, even for large external forces. Furthermore, when the applied pull-out forces are large (Figure 13b), we notice that the first loop in the GRM70/30 is wider, showing the increased damping because of the rubber in the GSI layer. The latter supports the results of the stochastic subspace identification method (Table 5) and the abrupt decay of the motion in the first cycle of oscillation shown in Figure 11c and d.

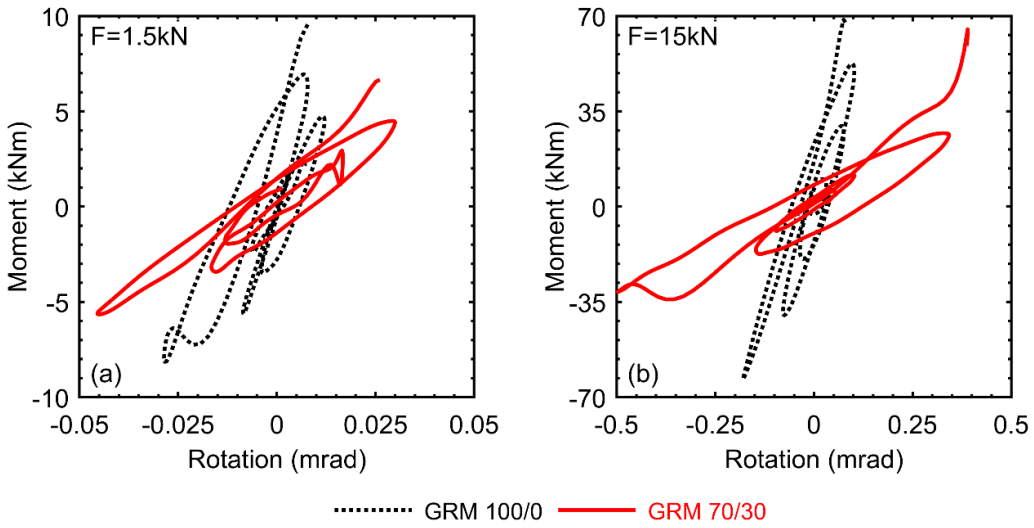

Figure 13 Moment versus foundation rotation loops for pull-out force (a) 1.5kN and (b) 15kN in the case of the GRM100/0 and GRM70/30 foundation soil.

Forced-vibration results

Figure 14 shows a time window of the recorded roof acceleration per shaker frequency during Experiment 3 when moderate to strong amplitude forces are applied to the structure placed on the three GSI mixtures (Table 4). The acceleration response for all the excitation frequencies is approximately identical as the structure vibrates on the GRM100/0 and GRM90/10. The motion is remarkably amplified for these two GRM when the input frequency is 4Hz, close to the fundamental natural frequency of the GSI-structure system, and its amplitude becomes two times the response at 3.5Hz. For larger input frequencies, the amplitude decreases until the shaker is set to operate at 7Hz. One should consider that when the excitation frequency is 4Hz, the loading force amplitude is 4.38kN in Experiment 3. In contrast, for the excitation frequency of 3.5Hz and 7Hz, the corresponding values are 3.35kN and 13.4kN, respectively (Figure 7b).

The measured acceleration in the GRM70/30 is larger for excitation frequencies close to 2.5Hz, in the vicinity of the GRM70/30-structure system fundamental natural frequency. For frequencies over 3.25Hz, the amplitude is significantly reduced compared to the GRM100/0- and GRM90/10-structure systems' response, stressing out the GRM rubber content's beneficial effect on the structure's response. We notice an average reduction of 40-60% in the frequency range of 4.5-7Hz in all the experiments. A similar average decrease was also seen for the same rubber proportion in soil-rubber mixture (SRM) layers studied as GSI in previous numerical and experimental reports [38,43].

At an operating frequency 9Hz during this test and at 8Hz in Experiment 4 (not shown here), we noticed an abrupt and unexpected amplification in the motion for the GRM70/30. The source seems to be related to a sharp increase in the movement's vertical and rocking components. However, further investigation is necessary on this incident before attempting any explanation.

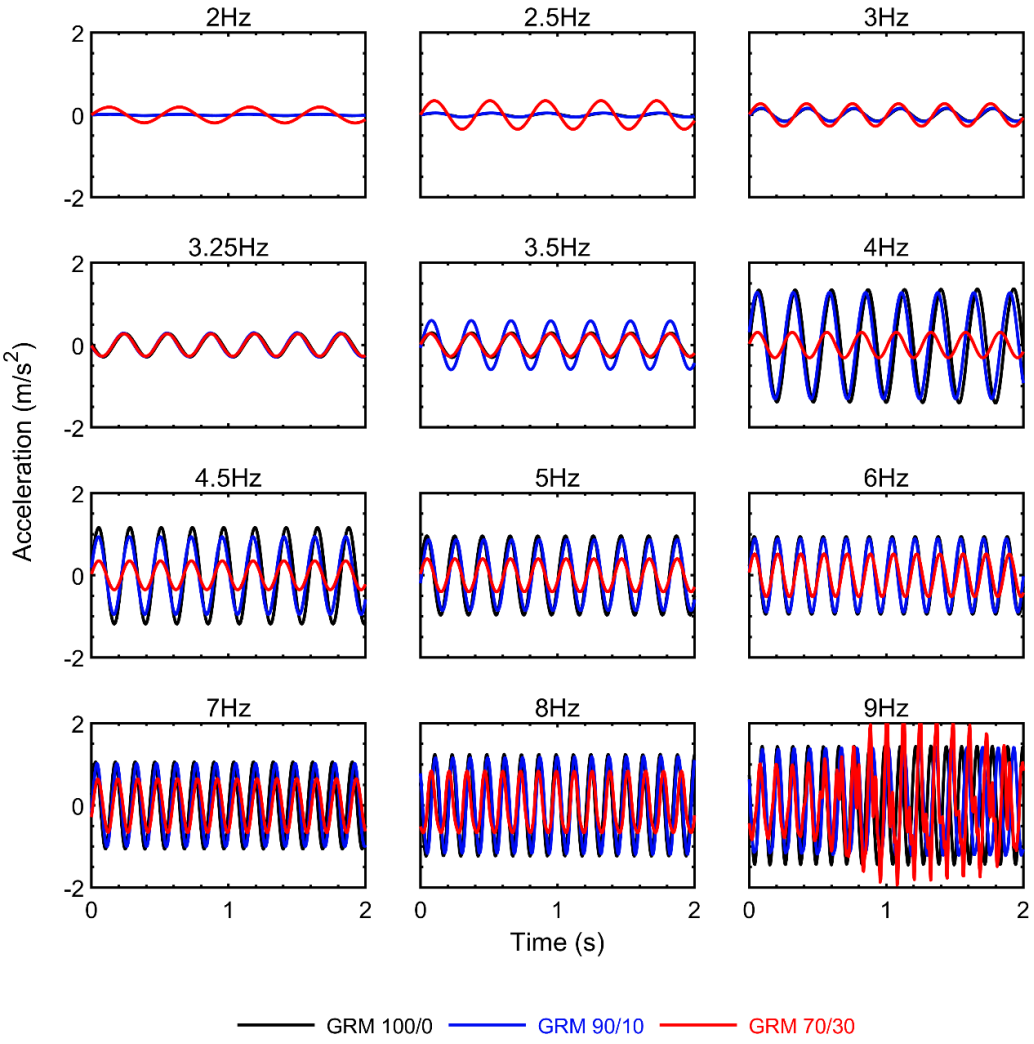

Figure 14 Recorded acceleration response histories at the roof for a wide range of excitation frequencies during the forced-vibration Experiment 3 (see Table 4).

Figures 15a and 15c present the peak acceleration amplitude recorded at the roof plotted against the shaker frequency for two forced-vibration tests. The peak amplitude was defined when the vibration of the structure reached the steady-state.

In Experiment 2, we applied low to moderate amplitude forces (Table 4) in a frequency range between 2 and 10Hz. The resonant frequency of the GSI-structure system for the benchmark test of the GRM100/0 layer is estimated between 4Hz and 4.5Hz. No significant difference is observed in the resonance when the structure is vibrating on the GRM90/10, corroborating the system identification results from the ambient noise measurements and the free-vibration tests. Similar conclusions are drawn from the plot of the acceleration response factor *Ra* versus the shaker frequency (Figures 15b and d). *Ra* is calculated as the ratio of the recorded acceleration at the roof over the shaker force divided by the superstructure mass [62].

In Experiment 4, the largest forces are applied to the structure in frequencies between 2 and 8Hz. The resonant frequency of the system shifts to 4Hz for both GRM100/0 and GRM90/10. On further examination, we see that the amplitude of accelerations for the same input frequency when the structure is founded on the GRM90/10 is slightly smaller than the GRM100/0, indicating a modest increase in the damping due to the presence of rubber in the GSI layer.

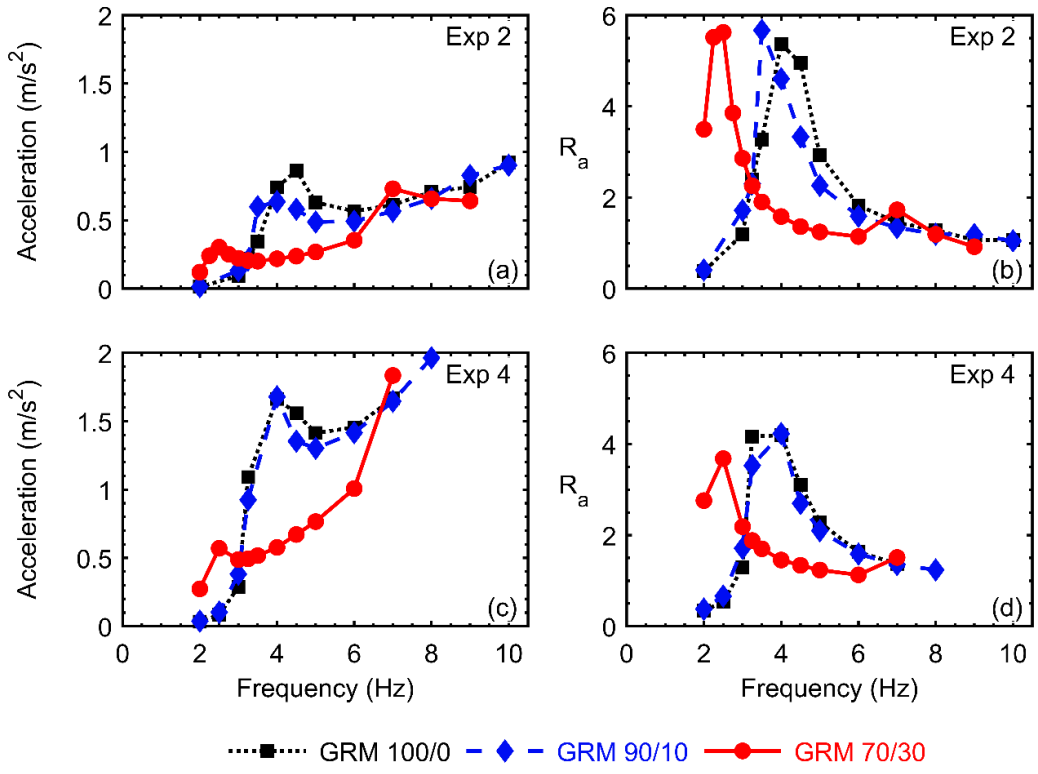

Figure 15 (a), (c) Maximum amplitude of the acceleration recorded at the roof and (b), (d) calculated transmissibility functions during the forced-vibration Experiment 2 and Experiment 4 at different excitation frequencies.

On the other hand, the resonant frequency of the structure resting on the GRM70/30 presents a pronounced shift to 2.5Hz in both Experiments 2 and 4, underlining the rubber's strong effect in the stiffness reduction of the GSI-structure system. The measured response and *Ra* values in the range 3-6Hz are much lower than the GRM100/0 layer, especially in Experiment 4, indicating a significant increase in the damping.

We explored the wave propagation in the soil by examining the motion's decay with increasing distance from the foundation slab. Figure 16 shows the maximum amplitude of the recorded velocity in the direction of loading on the soil surface when the structure was subjected to three harmonic sinusoidal forces at 2.5Hz, 4Hz, and 6Hz, during the forced-vibration Experiment 4.

We see a sharp 80% decrease of the motion at the top of the foundation (values at zero abscissae in the plots at distance B/6 (B equals the foundation width) when the foundation is lying over the GRM100/0 (Figure 16a and b), and the structure is excited at 6Hz. A slightly larger reduction is detected when the shaker frequency is 4Hz, closer to the system's resonant frequency. In contrast, for the smaller harmonic force at 2.5Hz, the reduction is even more considerable because of the lower force related to the lower excitation frequency. At a distance equal to 2B/3, the recorded velocity decrease is more than 93% for all the harmonic forces.

When the structure is placed on the GRM90/10 layer, the measured horizontal velocities are lower as the GSI contributes to the dissipation of a larger portion of energy (Figure 16c and d). The rubber's impact in the damping is even more pronounced in the case of the GRM70/30. The velocity at B/6 is reduced by more than 92% compared to the foundation motion and irrespectively of the shaker frequency, while at B/3, the response can be considered negligible (Figure 16e and f). This reduction means that, for all practical purposes, this GSI (GRM70/30) layer absorbs almost 100% of the outgoing energy for all excitation forces.

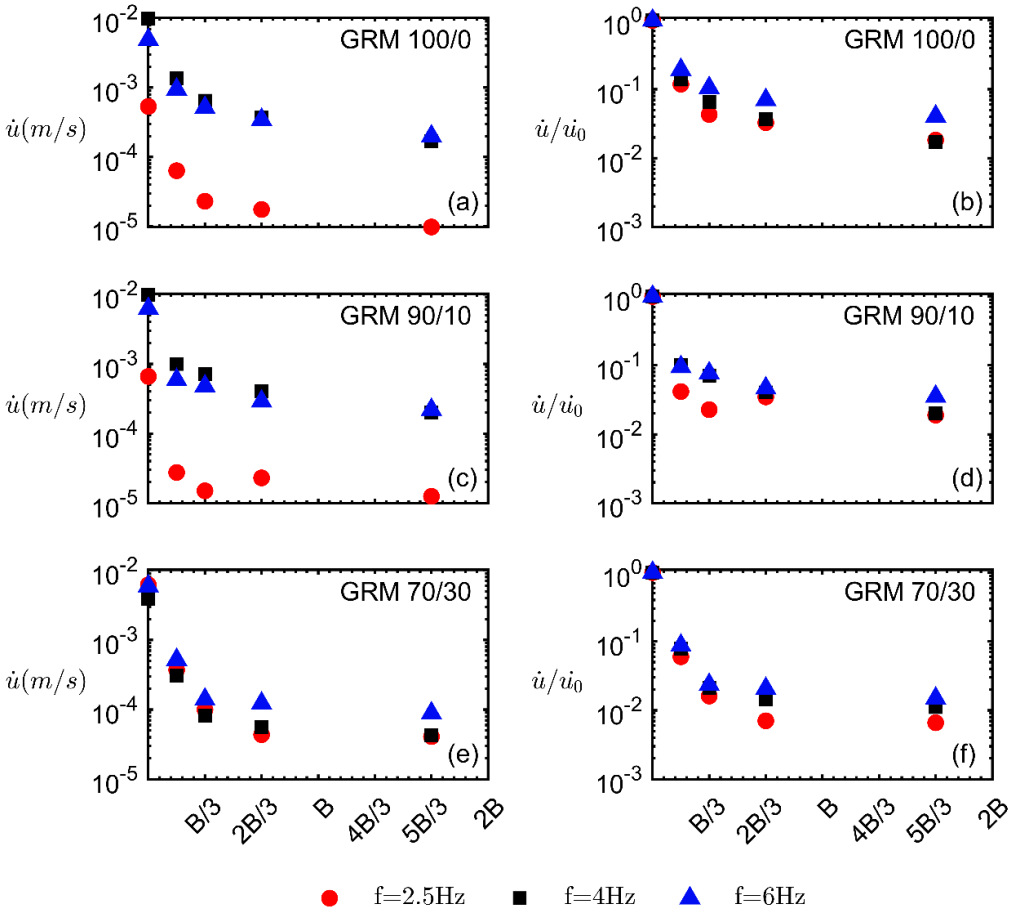

Figure 16 Decay of the soil surface horizontal velocity as recorded (a, c, e), and normalized by the velocity value recorded on the foundation (b, d, f) at increasing distance from the foundation slab, for the forced-vibration Experiment 4 and different excitation frequencies.

We investigated the decay of the motion inside the GRM by analyzing the uniaxial accelerometers' recordings and the SAAR sensors placed in the GRM immediately below the structure (Figure 8f). Figure 17 shows a time window of the recorded acceleration at three depths inside the GRM layers and the foundation recording for the GRM100/0 and the GRM70/30 during the excitation of the structure at 6Hz in Experiment 3. The recordings at the top of the foundation and 0.09m immediately below it are almost equal in both GRM cases. However, it is clearly shown that the motion reduces more than twice when at the bottom of the GRM70/30 layer compared to the GRM100/0 layer, signifying the effect of the increased material damping of the GRM due to the increased rubber content.

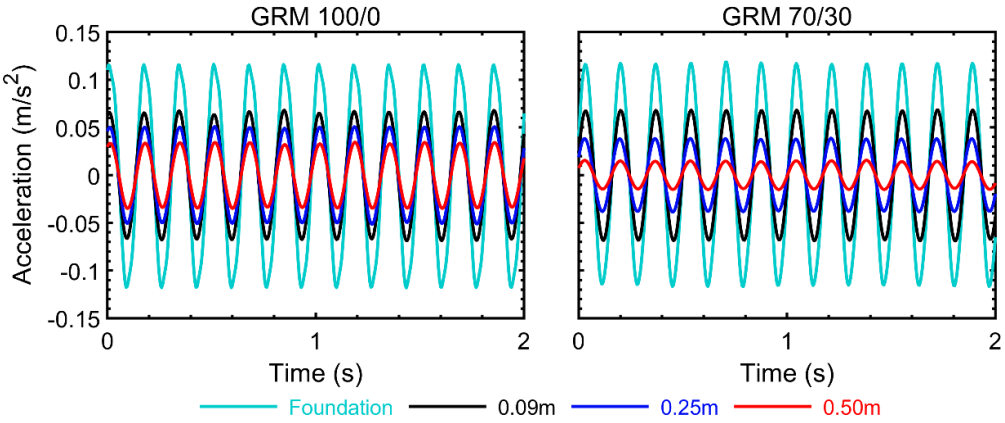

Figure 17 Acceleration response histories recorded at the top of the foundation and inside the GRM layers at three depths (0.09m, 0.25m, 0.5m) by the uniaxial accelerometers for excitation frequency 6Hz during the forced-vibration Experiment 3.

Figure 18 shows the maximum acceleration recorded in the GRM. Because the reinforced concrete foundation slab is rigid, at zero-depth, the value is equal to the recording at the top of the foundation during forced-vibration Experiment 4, when the structure was excited at 2.5Hz, 4Hz, and 6Hz. The grey area of each plot portrays the thickness of each GRM layer. It presents the corresponding maximum acceleration recorded at those depths by the uniaxial accelerometers (solid markers) and by the SAAR sensors (hollow markers), wherever available.

In the case of the GRM100/0 layer (Figure 18a and b), the acceleration at 0.25m depth (equal to B/12) is reduced by 50-60%. Moreover, the recording at the bottom of the GRM layer at a depth approximately equal to B/6 is decreased by about 75% from the top of the foundation. Besides, the recording below the mixture, at B/5, shows that the response reduces further by another 5-10%.

In the presence of only 10% rubber content per weight, the motion's attenuation becomes significantly greater (Figure 18c and d). Moreover, inside the GRM70/30 (Figure 18e and f), the acceleration at depth=B/12 reduces remarkably by almost 70% from the top of the foundation, whereas at the bottom of the GSI layer, the corresponding value decreases by over 90%. Finally, below the GRM layer, the response amplitude can be considered negligible for practical purposes. In conjunction with the recordings obtained on the soil surface (Figure 16), the latter suggests that the most considerable portion of the structure's energy transmitted into the soil is dissipated inside the GSI gravel-rubber mixture. Additionally, the decay of the motion with depth seems to be relatively independent of the excitation frequency. The beneficial effects of the gravel rubber mixture's improved dynamic parameters cover a wide frequency range of engineering interest.

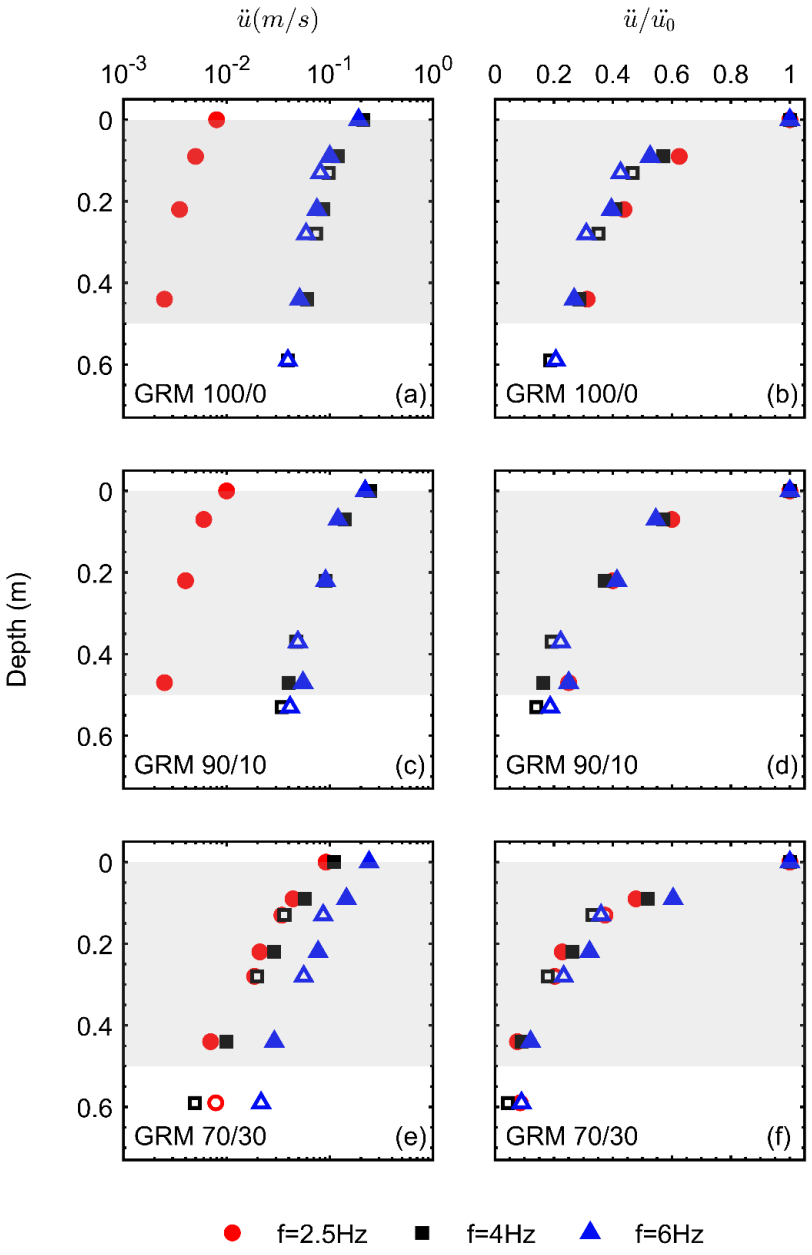

Figure 18 Decay of the motion with depth as recorded immediately below the structure inside and below the GRM layer (grey color hatch) (a, c, e) and normalized by the recording on the foundation in forced-vibration Experiment 4 (b, d, f). The value plotted at depth = 0m is recorded at the top of the foundation.

CONCLUSIONS

We performed and presented the first extensive experimental field campaign in the full-scale prototype structure of EuroProteas to investigate the potential of gravel rubber mixtures (GRM) as a means of geotechnical seismic isolation (GSI). The structure was placed on three GRM layers with different rubber content per mixture weight. A dense instrumentation scheme was designed and implemented to monitor the structure's response, the GRM layer, and the surrounding soil. Ambient noise measurements, free- and forced-vibration experiments were carried out to investigate the effect of the rubber content of the GRM layer on the dynamic response of the structure and examine the overall performance of the GRM as a GSI system in an actual structure.

Overall, our results showed that a geotechnical seismic isolation layer composed of a gravel-rubber mixture with 30% rubber content per weight effectively isolates the structure. Even 0.5m thickness (i.e., B/6 of the foundation width) of the GSI system is successfully cutting off practically all emitted waves at a (horizontal or vertical) distance of B/6 from the foundation, with B being the foundation width. In particular:

- For a GRM layer with low rubber content (10%), the alteration in the structure's dynamic characteristics is almost negligible, as shown in all the results. The fundamental frequency remains the same, and there is only a slight increase in the damping and a modest reduction in the structure's response when the excitation is small.
- For 30% rubber content, we notice a significant modification in the dynamic properties of the GSI-structure system, as its stiffness decreases and its damping increases.
- A generous increase in the rubber content reduces the lateral and rocking stiffness of the GSI-structure system and amplifies the structure's rocking response irrespectively of the excitation amplitude.
- For practical purposes, an upper bound of 30% rubber per mixture weight can be considered. Beyond that threshold, the mixture cannot be effectively compacted.
- A significant portion of the energy is dissipated in the GRM layer before its radiation to the surrounding soil, proclaiming the beneficial effects of the GRM as a geotechnical seismic isolation system of the structure.

ACKNOWLEDGMENTS

This study was performed in the framework of the Transnational Access Project "Soil Frame-Interaction Analysis through large-scale tests and advanced numerical finite element modeling" funded under the European project "Seismology and Earthquake Engineering Research Infrastructure Alliance for Europe – SERA-TA – H2020 (Grant Agreement 730900)". We want to acknowledge the contribution of OASP-ITSAK for providing us with part of the instrumentation and human resources to execute the tests. The help of Emmanuil Rovithis, Nikos Adam, Apostolos Marinos is greatly appreciated. We want to thank Christos Petridis, Maria Manakou, Angelos Tsinaris, and all the Research Unit of Soil Dynamics and Geotechnical Earthquake Engineering of AUTH for contributing to executing the tests successfully.

REFERENCES

1. Kelly JM. Base Isolation: Linear Theory and Design. *Earthquake Spectra* 1990; **6**(2): 223–244. DOI: 10.1193/1.1585566.
2. Naeim F, Kelly JM. *Design of Seismic Isolated Structures*. Hoboken, NJ, USA: John Wiley & Sons, Inc.; 1999. DOI: 10.1002/9780470172742.
3. Banović I, Radnić J, Grgić N. Geotechnical Seismic Isolation System Based on Sliding Mechanism Using Stone Pebble Layer: Shake-Table Experiments. *Shock and Vibration* 2019; **2019**: 1–26. DOI: 10.1155/2019/9346232.
4. Karatzetzou A, Pitilakis D. Modification of Dynamic Foundation Response Due to Soil-Structure Interaction. *Journal of Earthquake Engineering* 2018; **22**(5): 861–880. DOI: 10.1080/13632469.2016.1264335.
5. Karatzetzou A, Pitilakis D, Stefanidou S. Partitioning Displacement Demand of Flexible-base Structures because of SSI. *Journal of Earthquake Engineering* 2020: 1–18. DOI: 10.1080/13632469.2020.1772149.
6. Abate G, Massimino MR. Dynamic soil-structure interaction analysis by experimental and numerical modelling. *Rivista Italiana Di Geotecnica* 2016; **50**(2): 44–70.
7. Massimino MR, Abate G, Grasso S, Pitilakis D. Some aspects of DSSI in the dynamic response of fully-coupled soil-structure systems. *Rivista Italiana Di Geotecnica* 2019; **1**: 44–70.
8. Massimino MR, Abate G, Corsico S, Louarn R. Comparison Between Two Approaches for Nonlinear FEM Modelling of the Seismic Behaviour of a Coupled Soil–Structure System. *Geotechnical and Geological Engineering* 2019; **37**(3): 1957–1975. DOI: 10.1007/s10706-018-0737-y.
9. Trifunac MD, Todorovska MI. Nonlinear soil response as a natural passive isolation mechanism—the 1994 Northridge, California, earthquake. *Soil Dynamics and Earthquake Engineering* 1998; **17**(1): 41–51. DOI: 10.1016/S0267-7261(97)00028-6.
10. Anastasopoulos I, Gazetas G, Loli M, Apostolou M, Gerolymos N. Soil failure can be used for seismic protection of structures. *Bulletin of Earthquake Engineering* 2010; **8**(2): 309–326. DOI: 10.1007/s10518-009-9145-2.

11. Gazetas G. 4th Ishihara lecture: Soil-foundation-structure systems beyond conventional seismic failure thresholds. *Soil Dynamics and Earthquake Engineering* 2015; **68**: 23–39. DOI: 10.1016/j.soildyn.2014.09.012.
12. Massimino MR, Biondi G. Some experimental evidences on dynamic soil-structure interaction. *Proceedings of COMPDYN 2015 - 5th ECCOMAS Thematic Conference on Computational Methods in Structural Dynamics and Earthquake Engineering*, Crete Island: 2015.
13. Tsang H. Geotechnical seismic isolation. *Earthquake Engineering: New Research Nova Science Publishers, Inc, New York, US* 2009: 55–87.
14. ASTM. D6270-08 Standard practice for use of scrap tires in civil engineering applications 2008.
15. CEN/TS 14243. *Materials produced from end of life tyres-Specification of categories based on their dimension(s) and impurities and methods for determining their dimension(s) and impurities*. European Committee for Standardization (CEN), Brussels, Belgium: 2010.
16. Anastasiadis A, Senetakis K, Pitilakis K, Gargala C, Karakasi I, Edil TB, *et al.* Dynamic Behavior of Sand/Rubber Mixtures. Part I: Effect of Rubber Content and Duration of Confinement on Small-Strain Shear Modulus and Damping Ratio. *Journal of ASTM International* 2012; **9**(2): 103680. DOI: 10.1520/JAI103680.
17. Senetakis K, Anastasiadis A, Pitilakis K, Souli A, Edil TB, Dean SW. Dynamic Behavior of Sand/Rubber Mixtures, Part II: Effect of Rubber Content on G/GO-γ-DT Curves and Volumetric Threshold Strain. *Journal of ASTM International* 2012; **9**(2): 103711. DOI: 10.1520/JAI103711.
18. Senetakis K, Anastasiadis A, Pitilakis K. Dynamic properties of dry sand/rubber (SRM) and gravel/rubber (GRM) mixtures in a wide range of shearing strain amplitudes. *Soil Dynamics and Earthquake Engineering* 2012; **33**(1): 38–53. DOI: 10.1016/j.soildyn.2011.10.003.
19. Senetakis K, Anastasiadis A. Effects of state of test sample, specimen geometry and sample preparation on dynamic properties of rubber–sand mixtures. *Geosynthetics International* 2015; **22**(4): 301–310. DOI: 10.1680/gein.15.00013.
20. Pistolas GA, Anastasiadis A, Pitilakis K. Dynamic Behaviour of Granular Soil Materials Mixed with Granulated Rubber: Effect of Rubber Content and Granularity on the Small-Strain Shear Modulus and Damping Ratio. *Geotechnical and Geological Engineering* 2017; **36**(2): 1267–1281. DOI: 10.1007/s10706-017-0391-9.
21. Pistolas GA, Anastasiadis A, Pitilakis K. Dynamic behaviour of granular soil materials mixed with granulated rubber: influence of rubber content and mean grain size ratio on shear modulus and damping ratio for a wide strain range. *Innovative Infrastructure Solutions* 2018; **3**(1): 1–14. DOI: 10.1007/s41062-018-0156-1.
22. Tsinaris A, Anastasiadis A, Pitilakis K. Numerical investigation of improving the seismic response of retaining structures by using lightweight mixtures as backfill material. *Proceedings of the 16th European Conference on Earthquake Engineering*, Thessaloniki: 2018.
23. Edil TB, Bosscher PJ. Engineering Properties of Tire Chips and Soil Mixtures. *Geotechnical Testing Journal* 1994; **17**(4): 453. DOI: 10.1520/GTJ10306J.
24. Bosscher PJ, Edil TB, Kuraoka S. Design of Highway Embankments Using Tire Chips. *Journal of Geotechnical and Geoenvironmental Engineering* 1997; **123**(4): 295–304. DOI: 10.1061/(ASCE)1090-0241(1997)123:4(295).
25. Lee JH, Salgado R, Bernal A, Lovell CW. Shredded Tires and Rubber-Sand as Lightweight Backfill. *Journal of Geotechnical and Geoenvironmental Engineering* 1999; **125**(2): 132–141. DOI: 10.1061/(ASCE)1090-0241(1999)125:2(132).
26. Argyroudis S, Palaiochorinou A, Mitoulis S, Pitilakis D. Use of rubberised backfills for improving the seismic response of integral abutment bridges. *Bulletin of Earthquake Engineering* 2016; **14**(12): 3573–3590. DOI: 10.1007/s10518-016-0018-1.
27. Hazarika H, Kohama E, Sugano T. Underwater Shake Table Tests on Waterfront Structures Protected with Tire Chips Cushion. *Journal of Geotechnical and Geoenvironmental Engineering* 2008; **134**(12): 1706–1719. DOI: 10.1061/(ASCE)1090-0241(2008)134:12(1706).
28. Edincliler A. Using waste tire-soil mixtures for embankment construction. *Proceedings of the international workshop on scrap tire derived geomaterials—opportunities and challenges, Yokosuka, Japan*, 2007.
29. Edil TB. A Review of Mechanical and Chemical Properties of Shredded Tires and Soil Mixtures. *Recycled Materials in Geotechnics*, Reston, VA: American Society of Civil Engineers; 2004. DOI: 10.1061/40756(149)1.
30. Karmokar A. Use of scrap tire derived shredded geomaterials in drainage application. *Proceedings of the international workshop on scrap tire derived geomaterials—opportunities and challenges, Yokosuka, Japan*,

2007.
31. Tsang H. Seismic isolation by rubber–soil mixtures for developing countries. *Earthquake Engineering & Structural Dynamics* 2008; **37**(2): 283–303. DOI: 10.1002/eqe.756.
32. Dhanya JS, Boominathan A, Banerjee S. Response of low-rise building with geotechnical seismic isolation system. *Soil Dynamics and Earthquake Engineering* 2020; **136**: 106187. DOI: 10.1016/j.soildyn.2020.106187.
33. Pistolas GA, Pitilakis K, Anastasiadis A. A numerical investigation on the seismic isolation potential of rubber/soil mixtures. *Earthquake Engineering and Engineering Vibration* 2020; **19**(3): 683–704. DOI: 10.1007/s11803-020-0589-3.
34. Mavronicola E, Komodromos P, Charmpis DC. Numerical Investigation of Potential Usage of Rubber-Soil Mixtures as a Distributed Seismic Isolation Approach. *Civil-Comp Proceedings*, vol. 93, Civil-Comp Press; 2010. DOI: 10.4203/ccp.93.168.
35. Tsang H, Lo SH, Xu X, Neaz Sheikh M. Seismic isolation for low-to-medium-rise buildings using granulated rubber-soil mixtures: numerical study. *Earthquake Engineering & Structural Dynamics* 2012; **41**(14): 2009–2024. DOI: 10.1002/eqe.2171.
36. Pitilakis K, Karapetrou S, Tsagdi K. Numerical investigation of the seismic response of RC buildings on soil replaced with rubber–sand mixtures. *Soil Dynamics and Earthquake Engineering* 2015; **79**: 237–252. DOI: 10.1016/j.soildyn.2015.09.018.
37. Brunet S, de la Llera JC, Kausel E. Nonlinear modeling of seismic isolation systems made of recycled tire-rubber. *Soil Dynamics and Earthquake Engineering* 2016; **85**: 134–145. DOI: 10.1016/j.soildyn.2016.03.019.
38. Tsang H, Pitilakis K. Mechanism of geotechnical seismic isolation system: Analytical modeling. *Soil Dynamics and Earthquake Engineering* 2019; **122**(February): 171–184. DOI: 10.1016/j.soildyn.2019.03.037.
39. Kaneko T, Orense RP, Hyodo M, Yoshimoto N. Seismic Response Characteristics of Saturated Sand Deposits Mixed with Tire Chips. *Journal of Geotechnical and Geoenvironmental Engineering* 2013; **139**(4): 633–643. DOI: 10.1061/(ASCE)GT.1943-5606.0000752.
40. Xiong W, Yan MR, Li YZ. Geotechnical Seismic Isolation System - Further Experimental Study. *Applied Mechanics and Materials* 2014; **580**–**583**: 1490–1493. DOI: 10.4028/www.scientific.net/AMM.580-583.1490.
41. Bandyopadhyay S, Sengupta A, Reddy GR. Performance of sand and shredded rubber tire mixture as a natural base isolator for earthquake protection. *Earthquake Engineering and Engineering Vibration* 2015; **14**(4): 683–693. DOI: 10.1007/s11803-015-0053-y.
42. Tsiavos A, Alexander NA, Diambra A, Ibraim E, Vardanega PJ, Gonzalez-Buelga A, *et al.* A sand-rubber deformable granular layer as a low-cost seismic isolation strategy in developing countries: Experimental investigation. *Soil Dynamics and Earthquake Engineering* 2019; **125**: 105731. DOI: 10.1016/j.soildyn.2019.105731.
43. Tsang H, Tran D, Hung W, Pitilakis K, Gad EF. Performance of geotechnical seismic isolation system using rubber-soil mixtures in centrifuge testing. *Earthquake Engineering & Structural Dynamics* 2020(October): eqe.3398. DOI: 10.1002/eqe.3398.
44. Mahdavisefat E, Salehzadeh H, Heshmati AA. Full-scale experimental study on screening effectiveness of SRM-filled trench barriers. *Géotechnique* 2018; **68**(10): 869–882. DOI: 10.1680/jgeot.17.P.007.
45. Pitilakis D, Rovithis E, Anastasiadis A, Vratsikidis A, Manakou M. Field evidence of SSI from full-scale structure testing. *Soil Dynamics and Earthquake Engineering* 2018; **112**: 89–106. DOI: 10.1016/j.soildyn.2018.04.024.
46. Vratsikidis A, Pitilakis D. Full-scale free-and forced-vibration experiments at the EuroProteas SSI facility: experimental data exploitation. *Proceedings of the 16th European Conference on Earthquake Engineering*, Thessaloniki: 2018.
47. Pitilakis K, Raptakis D, Lontzetidis K, Tika-Vassilikou T, Jongmans D. Geotechnical and geophysical description of EURO-SEISTEST, using field, laboratory tests and moderate strong motion recordings. *Journal of Earthquake Engineering* 1999; **3**(03): 381–409.
48. Manakou MV, Raptakis D, Chávez-García FJ, Apostolidis PI, Pitilakis K. 3D soil structure of the Mygdonian basin for site response analysis. *Soil Dynamics and Earthquake Engineering* 2010; **30**(11): 1198–1211. DOI: 10.1016/j.soildyn.2010.04.027.
49. Masad E, Taha R, Ho C, Papagiannakis T. Engineering properties of tire/soil mixtures as a lightweight fill material. *Geotechnical Testing Journal* 1996; **19**(3): 297–304. DOI: 10.1520/gtj10355j.

50. Zornberg JG, Cabral AR, Viratjandr C. Behaviour of tire shred - Sand mixtures. *Canadian Geotechnical Journal* 2004; **41**(2): 227–241. DOI: 10.1139/t03-086.
51. Anastasiadis A, Senetakis K, Pitilakis K. Small-Strain Shear Modulus and Damping Ratio of Sand-Rubber and Gravel-Rubber Mixtures. *Geotechnical and Geological Engineering* 2012; **30**(2): 363–382. DOI: 10.1007/s10706-011-9473-2.
52. Kim HK, Santamarina JC. Sand–rubber mixtures (large rubber chips). *Canadian Geotechnical Journal* 2008; **45**(10): 1457–1466. DOI: 10.1139/T08-070.
53. ASTM. D854-02 Standard Test Methods for Specific Gravity of Soil Solids by Water Pycnometer 2002. DOI: 10.1520/D0854-02.
54. Pistolas GA. Experimental and numerical investigation of the implementation of recycled materials mixtures in the foundation of structures for the improvement of seismic behaviour, Phd Dissertation (in Greek). Department of Civil Engineering, Aristotle University of Thessaloniki, 2015.
55. ASTM. C136 / C136M - 19 Standard Test Method for Sieve Analysis of Fine and Coarse Aggregates 2019.
56. ASTM. D2487 - 17e1 Standard Practice for Classification of Soils for Engineering Purposes (Unified Soil Classification System) 2017.
57. ASTM. D6270 - 98 Standard Practice for Use of Scrap Tires in Civil Engineering Applications 1998.
58. Boore DM, Bommer JJ. Processing of strong-motion accelerograms: needs, options and consequences. *Soil Dynamics and Earthquake Engineering* 2005; **25**(2): 93–115. DOI: 10.1016/j.soildyn.2004.10.007.
59. Reynders E, Schevenels M, De Roeck G. MACEC 3.2: A Matlab toolbox for experimental and operational modal analysis. *Department of Civil Engineering, KU Leuven* 2014.
60. Tileylioglu S, Stewart JP, Nigbor RL. Dynamic Stiffness and Damping of a Shallow Foundation from Forced Vibration of a Field Test Structure. *Journal of Geotechnical and Geoenvironmental Engineering* 2011; **137**(4): 344–353. DOI: 10.1061/(ASCE)GT.1943-5606.0000430.
61. Star LM, Tileylioglu S, Givens MJ, Mylonakis G, Stewart JP. Evaluation of soil-structure interaction effects from system identification of structures subject to forced vibration tests. *Soil Dynamics and Earthquake Engineering* 2019; **116**(September 2018): 747–760. DOI: 10.1016/j.soildyn.2018.09.038.
62. Chopra AK. *Dynamics of structures, Theory and Applications to Earthquake Engineering*. (4th edition) Pearson Education Upper Saddle River, NJ; 2012.